Journal of Materials Science and Engineering A 15 (4-6) (2025) 44-54
doi: 10.17265/2161-6213/2025.4-6.002

Adsorption Kinetics, Mechanisms, and Performance of Mango Peel, Seed Shell, and Kernel Biosorbents for Methyl Red and Cu (II) Removal

Adatz Jean Claude Jean Claude De Tout[1], Bike Mbah Jean Baptiste[2], Taybe Ngaba[3], Alang Micheal Bong[2], Fognaba Honoré[1], Tekoumbo Tedontsa Larissa Canuala[2], Noumi Guy Bertrand[1]

1. Department of Chemistry, Faculty of Sciences, University of Ngaoundere, Ngaoundere, Cameroon

2. Department of Applied Chemistry, National School of Agro-Industrial Sciences, University of Ngaoundere, Ngaoundere, Cameroon

3. Department of Civil Engineering, Building Materials and Architecture, National Polytechnic School, University of Maroua, Maroua, Cameroon

Abstract: This study investigates the adsorption performance and underlying mechanisms of mango waste-derived biosorbents, including peels, seed shells, and kernels, for the simultaneous removal of methyl red (MR) and Cu(II) ions from aqueous solutions. The morphological, physicochemical, and structural properties of the residues were characterized, revealing a high lignocellulosic content, abundant functional groups (hydroxyl, carboxyl, phenolic, and amine), and structural features favorable for adsorption. Adsorption kinetics were evaluated using intraparticle diffusion, pseudo-first-order, and pseudo-second-order models, indicating that the process is primarily governed by chemisorption and surface interactions, with multiple stages including surface adsorption and pore diffusion. Intraparticle diffusion analysis confirmed that both boundary layer and pore diffusion contribute to the overall adsorption rate. FTIR and Boehm titration analyses suggested that the adsorption mechanisms involve electrostatic interactions, hydrogen bonding, ion exchange, and surface complexation. Among the biosorbents, mango kernels exhibited the highest adsorption capacities for both MR and Cu(II), highlighting their potential as low-cost and sustainable materials for water treatment. These findings provide new insights into the valorization of mango residues as multifunctional biosorbents for environmental remediation applications.

Keywords: Mango residues, biosorbent, methyl red, copper ions, adsorption kinetics, mechanism, lignocellulosic materials.

1. Introduction

The discharge of untreated industrial wastewater, particularly from textile, chemical, and metallurgical sectors, continues to introduce hazardous pollutants such as synthetic dyes and heavy metals into aquatic ecosystems. Among these contaminants, methyl red and copper (II) ions are of particular concern due to their toxicity, persistence, and resistance to biodegradation, posing serious risks to aquatic life and human health. With over 70% of global wastewater still released without adequate treatment, the development of efficient and sustainable remediation technologies remains a critical environmental priority [1, 2].

Among the available treatment methods, adsorption has emerged as one of the most promising due to its cost-effectiveness, operational simplicity, and environmental compatibility. Conventional adsorbents, such as activated carbon, are widely used owing to their high surface area and sorption capacity, yet their elevated production cost and limited reusability constrain large-scale applications [3, 4]. Consequently, growing attention has been directed toward biosorbents derived from renewable and low-cost materials, particularly agricultural and agro-industrial wastes rich in lignocellulosic compounds (cellulose, hemicellulose, and lignin) [5, 6].

Corresponding author: Bike Mbah Jean Baptiste, Ph.D., associate professor, research fields: materials sciences, industrials processes, environmental protection.

In this context, mango (*Mangifera indica*) residues such as peels, seed shells, and kernels represent an abundant and underutilized biomass resource. Their porous structure, high surface reactivity, and diverse functional groups (–OH, –COOH, –C=O, and –NH_2) make them suitable candidates for adsorption processes [7-9]. Recent research has explored the potential of these residues for removing dyes [10, 11] and heavy metals [12, 13], demonstrating significant sorption capacities. However, most of these studies have been limited to single-pollutant systems or focused on individual residues under differing experimental conditions, which hinders direct comparison and practical applicability. Moreover, real wastewater systems typically contain multiple contaminants, where competitive adsorption phenomena significantly influence removal efficiency [14, 15].

Accordingly, the present study aims to valorize mango peel, seed shell, and kernel residues as efficient biosorbents for wastewater purification. The specific objectives are to:

- characterize the physicochemical properties of each mango residue;
- evaluate and compare the adsorption performance of each biosorbent for the simultaneous removal of methyl red and Cu(II) ions from aqueous solution; and
- elucidate the adsorption mechanisms using kinetic modeling (pseudo-first-order, pseudo-second-order, and intraparticle diffusion models).

This research contributes to sustainable waste management and the circular bioeconomy by promoting the conversion of agro-residues into high-value materials for environmental remediation.

2. Materials and Methods

2.1 Materials

Mango fruits of the *Mangifera indica* "Miami Late" variety were used in this study, together with analytical-grade methyl red ($C_{15}H_{15}N_3O_2$) and copper(II) sulfate pentahydrate ($CuSO_4 \cdot 5H_2O$). The mangoes were harvested from an orchard located in the Dang area (Ngaoundéré III District, Adamawa Region, Cameroon). After harvesting, the fruits were processed to recover three distinct residues: peels, seed shells, and kernels, which were subsequently employed for biosorbent preparation.

Stock solutions of methyl red and Cu(II) were prepared by dissolving the respective reagents in distilled water and then diluted to the desired working concentrations. These solutes were selected as representative organic (azo dye) and inorganic (heavy metal) pollutants for the adsorption study, owing to their prevalence in textile and electroplating effluents.

2.2 Methods

2.2.1 Morphological Characterization and Pretreatment of Mango Residues

Morphological characterization aimed to quantify the proportion and dimensions of mango residues, including the peel, seed shell, and kernel. Parameters such as length, thickness, and weight were measured using a ROCH France caliper (± 0.01 cm) and a SARTORIUS analytical balance (± 0.01 g).

Each fruit was washed twice with tap water to remove surface impurities, then characterized individually. The whole fruit was first weighed, and its length and width recorded. The peel was carefully removed, collected, and weighed. The pulp and husk were separated, and the husk was cracked open to isolate the seed shell and kernel, which were weighed separately to determine the distribution of the fruit's components.

For pretreatment, the residues were dried in a ventilated oven at 40–50°C to constant weight to preserve their chemical integrity. The dried samples were then ground using a FRITSCH industrial shredder (Model 86580, Idar-Oberstein, Germany) and homogenized manually in a porcelain mortar to obtain particles with an average size of about 3 mm. The powders were stored in airtight polyethylene containers under low-humidity conditions prior to analysis.

2.2.2 Evaluation of the Adsorption Potential of Mango Residues

Physicochemical and surface characterizations were performed to assess the adsorption potential of the mango residues. Moisture, volatile matter, ash, and fixed carbon contents were determined by standard gravimetric procedures (ASTM D3173–3175).

The structural composition (cellulose, hemicellulose, lignin, and extractives) was determined following classical acid hydrolysis and solvent extraction protocols [16, 17].

Surface functional groups were identified by Boehm titration, which quantifies acidic and basic surface sites via neutralization reactions with NaOH, Na_2CO_3, and $NaHCO_3$ solutions.

Fourier-transform infrared (FTIR) spectroscopy (400–4000 cm^{-1}, KBr pellet method) was used to identify the main surface functional groups responsible for adsorption interactions.

These analyses provided a comprehensive understanding of the structural and surface characteristics influencing adsorption performance.

2.2.3 Preparation of Mango Residue-based Biosorbents

Biosorbents were produced from mango peel, seed shell, and kernel through chemical activation using phosphoric acid. An 8 M H_3PO_4 solution was prepared by dilution of 95% concentrated acid with distilled water.

For impregnation, 100 g of raw residue were mixed with 1000 mL of the acid solution under magnetic stirring (100 rpm, 2 h). The slurry was then left to stand for complete impregnation. After activation, the material was washed repeatedly with distilled water until neutral pH was reached and dried at 50 °C to constant weight.

The dried biosorbents were ground and sieved to 1 mm particle size and labeled as MKB, MSB and MPB, respectively for mango kernel biosorbent, mango seed biosorbent and mango peel biosorbent. This phosphoric acid activation process enhances porosity and exposes oxygenated functional groups, thereby improving sorption capacity [18].

2.2.4 Kinetic Study of Simultaneous Adsorption of Methyl Red and Cu(II)

Batch kinetic experiments were carried out at 25±1°C under continuous agitation. A 30 mL binary solution containing equimolar concentrations of methyl red (MR) and Cu(II) (total: 25 $mg \cdot L^{-1}$, pH 4.5) was contacted with 0.05 g of biosorbent (MKB, MSB or MPB). Samples were collected at predetermined time intervals (0–60 min) and filtered before analysis. The residual MR concentration was measured at 522 nm and Cu(II) at 625 nm using a UV–Vis spectrophotometer (Shimadzu UV-1800).

The amount adsorbed (q, $\mu mol \cdot g^{-1}$) was calculated using:

$$q = \frac{(C_0 - C_t)}{m} * V \quad (1)$$

where C_0 and C_t ($\mu mol \cdot L^{-1}$) are the initial and time-dependent concentrations of solute, V (L) is the volume of solution, and m (g) is the mass of biosorbent.

3. Results and Discussion

3.1 Morphological Properties of the Mangifera Indica "Miami Late" Variety

The morphological features of the *Mangifera indica* "Miami Late" mango, harvested in the Dang locality (Cameroon), were analyzed based on its constituent parts: peel, pulp, seed shell, and kernel. Key dimensional and mass parameters are presented in Table 1.

The Miami Late mango exhibits an ovoid morphology, with an average length of 9.73 ± 4.08 cm, a thickness of 7.62 ± 0.51 cm, and an average mass of 279.16 ± 45.55 g. The edible pulp constitutes the majority of the fruit's mass (67.07%), while the combined residues—peel, seed shell, and kernel—account for approximately one-third (32.7%).

This high residue proportion underscores the potential for valorizing these by-products. Previous studies have reported comparable residue fractions for other mango varieties, confirming their relevance as renewable precursors for bio-based adsorbents [19-21]

Table 1 Morphological characteristics of the Miami Late mango.

Parameter	Average value	Proportion (%)
Length (cm)	9.73 ± 4.08	/
Thickness (cm)	7.62 ± 0.51	/
Mango mass (g)	279.16 ± 45.55	/
Pulp mass (g)	187.26 ± 39.19	67.07
Peel mass (g)	42.21 ± 5.40	15.12
Husk mass (g)	49.29 ± 7.22	17.65
Seed shell mass (g)	19.56 ± 2.32	7.00
Kernel mass (g)	29.73 ± 3.26	10.64
Total mass of residues (g)	91.15 ± 7.52	/

Table 2 Physicochemical properties, structural and elemental composition of mango residues.

Parameter	Mango Peels	Mango Seed	Mango Kernels
Physicochemical properties (%)			
Water content	74.12 ± 1.43	48.56 ± 1.82	67.95 ± 1.32
Dry matter content	25.88 ± 1.29	51.44 ± 1.42	32.05 ± 1.83
Ash content	5.65 ± 0.69	1.54 ± 0.23	3.57 ± 0.45
Volatile matter	73.64 ± 0.47	72.71 ± 0.38	66.67 ± 0.29
Fixed carbon	20.71 ± 0.16	25.75 ± 0.21	29.76 ± 0.18
Structural composition (%)			
Cellulose	27.54 ± 1.55	26.60 ± 1.43	28.64 ± 1.76
Hemicellulose	36.98 ± 1.23	39.31 ± 1.47	36.76 ± 1.53
Lignin	25.67 ± 0.72	30.83 ± 0.93	22.63 ± 0.58
Extractable	9.53 ± 0.43	2.76 ± 0.51	6.48 ± 0.32
Chemical Composition (%)			
Carbon	49.22	47.90	45.96
Hydrogen	3.54	6.20	5.30
Oxygen	45.91	46.13	46.41
Nitrogen	1.33	0.09	2.33

Values are expressed as mean ± standard deviation

However, their suitability as biosorbents depends strongly on their intrinsic physicochemical and structural properties, as discussed below.

3.2 Adsorption Potential of Mango Residues

3.2.1 Physicochemical Properties and Structural Composition

The physicochemical and structural profiles of mango peels, seed shells, and kernels are summarized in Table 2.

All residues display high water and volatile matter contents, reflecting their organic nature and porosity, both favorable for adsorption. Seed shells exhibit the highest dry matter and fixed carbon content, suggesting a denser, lignin-rich matrix that could enhance surface stability and adsorption performance [3, 18].

The residues are dominantly lignocellulosic, with cellulose, hemicellulose, and lignin contributing over 70% of their dry mass. The high lignin content in seed shells (30.83%) indicates strong aromatic and phenolic structures, which favor interactions with metal ions and aromatic dyes through π–π stacking and hydrogen bonding [5]. Conversely, the higher nitrogen and extractive contents in kernels may result from proteinaceous components, introducing amine and amide groups that can enhance complexation with cationic pollutants.

Elemental analysis corroborates the typical C–O–H–N composition of lignocellulosic biomass. The

Table 3 Surface functional group densities (meq g^{-1}) of mango residues.

Functional groups (meq/g)	Peels	Seed shell	Kernels
Carboxylic	2.30	1.20	1.05
Lactonic	1.75	0.30	0.28
Phenolic	2.85	3.15	2.26
Total acids	6.90	4.65	3.59
Total bases	2.27	3.29	5.40

nitrogen-rich composition of kernels (2.33%) may contribute to surface basicity and potential amphoteric behavior, supporting both cationic and anionic pollutant adsorption [6].

3.2.2 Surface Properties of Mango Residues

3.2.2.1 Surface Functional Group Densities

Surface acidity and basicity, determined via Boehm titration, are presented in Table 3.

All residues exhibit a predominance of acidic functional groups, primarily carboxylic and phenolic moieties. Peels show the highest total acidity (6.90 meq g^{-1}), consistent with their higher oxygen content and abundance of hydroxyl and carbonyl groups. In contrast, kernels display greater total basicity (5.40 meq g^{-1}), likely due to nitrogen-containing functionalities. Such balanced surface chemistries suggest diverse adsorption mechanisms encompassing both electrostatic and coordination interactions.

Similar acidity/basicity ratios have been reported for mango peel–based biosorbents by [15, 21], confirming their versatility for multi-pollutant adsorption.

3.2.2.2 FTIR Analysis of Functional Groups

FTIR spectra of the mango residues (Fig. 1) reveal characteristic absorption bands corresponding to hydroxyl, carboxyl, phenolic, ketonic, ester, ether, and amine groups, confirming their complex lignocellulosic composition.

A broad band at 3500–3300 cm^{-1} is assigned to O–H stretching vibrations from hydroxyl groups and adsorbed water. Peaks at 2920–2850 cm^{-1} indicate C–H stretching of aliphatic structures from cellulose and lignin. The strong band near 1730–1650 cm^{-1} corresponds to C=O stretching in carboxylic acids and esters, while the peak at 1634 cm^{-1} is associated with N–H bending of amine groups.

Bands at 1575 cm^{-1} and 1200 cm^{-1} correspond to aromatic ring vibrations and C–O–C stretching of ethers, respectively, while the prominent peak at ~1035 cm^{-1} is attributed to C–O stretching of alcohols or polysaccharides.

These findings corroborate the presence of functional groups responsible for adsorption via electrostatic attraction, hydrogen bonding, ion exchange, and complexation [20, 22, 23].

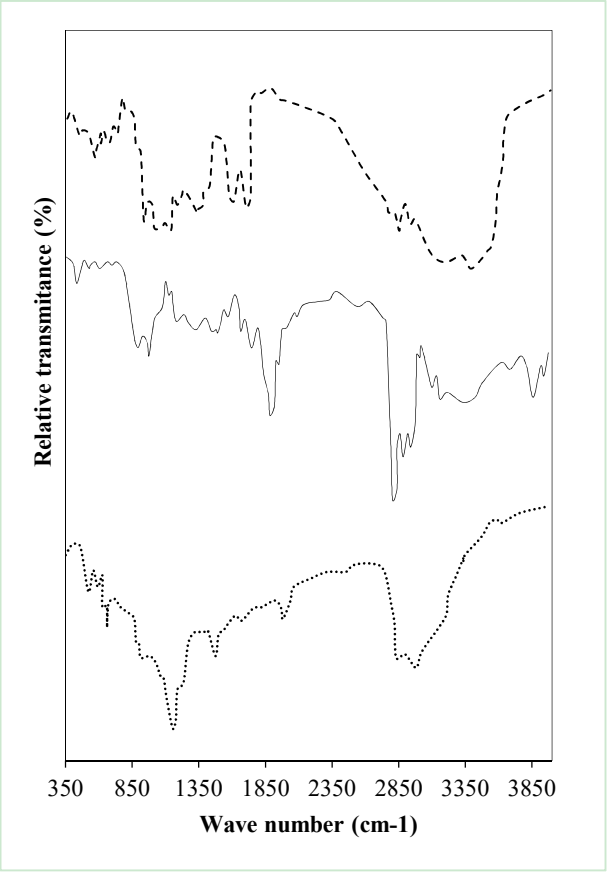

Fig. 1 FTIR spectra of mango residues: peel (---), seed shell (⋯⋯) and kernel (—).

4. Kinetic Study of Simultaneous Adsorption of Methyl Red and Cu(II) Ions by Biosorbents from Mango Peels, Seed Shells, and Kernels

Fig. 2 shows the adsorption kinetics of methyl red (MR) and Cu(II) onto mango-based biosorbents (MKB, MSB, and MPB). In all cases, adsorption was rapid during the first 10–15 minutes and reached equilibrium within 30 minutes, reflecting a typical biphasic kinetic pattern. This biphasic kinetic behavior reflects an initial phase driven by the abundance of active sites and a subsequent phase limited by sites saturation.

For each biosorbent, Cu(II) exhibited significantly higher uptake than MR across all biosorbents, likely due to its stronger affinity for oxygenated surface groups and possible steric hindrance limiting MR diffusion.

Among the biosorbents, MKB showed the highest adsorption capacities for both Cu(II) (~70 μmol/g) and MR (~32 μmol/g), followed by MSB and MPB. The superior performance of MKB is linked to its relatively high fixed carbon content (29.76%) and elevated density of basic surface functional groups (5.40 meq/g), which enhance complexation and ion exchange with metal cations [15].

MSB displayed intermediate adsorption performance consistent with its moderate lignin content (30.83%) and balanced surface functional group densities (acidic groups: 4.65 meq/g; basic groups: 3.29 meq/g). MPB, characterized by the highest density of acidic groups (6.90 meq/g) and the greatest water content (74.12%), exhibited competitive adsorption of methyl red due to strong interactions between acidic functional groups and the organic dye molecules. However, its lower basic group density (2.27 meq/g) and high water content likely limited its Cu(II) adsorption capacity [24].

Overall, the adsorption behavior reflects the combined influence of surface functional groups, structural composition, and moisture content of the biosorbents.

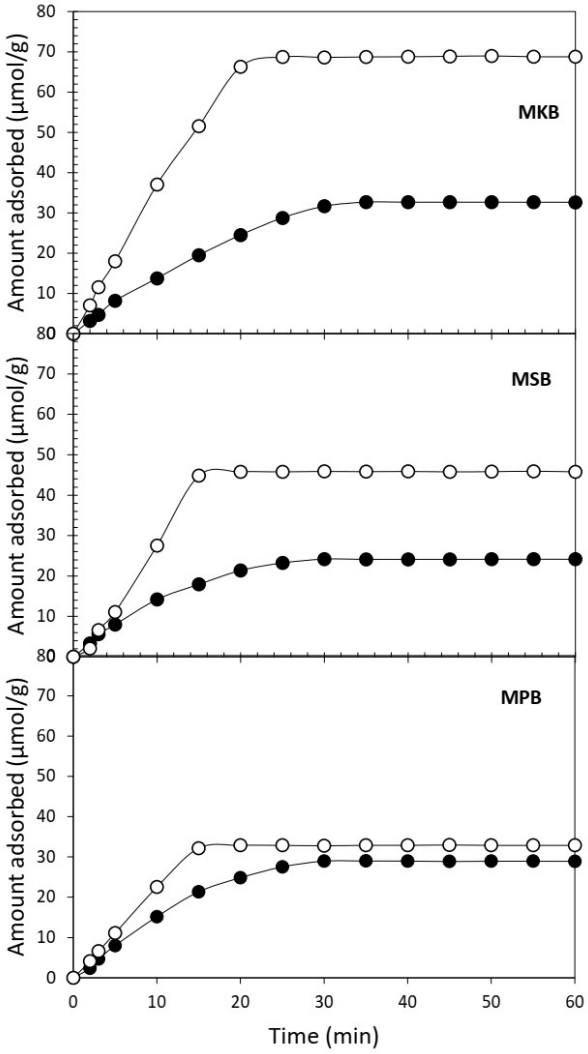

Fig. 2 Adsorption kinetics of methyl red (●) and Cu(II) (○) by mango kernels biosorbent (MKB), mango seed biosorbent (MSB) and mango peel biosorbent (MPB).

5. Adsorption Kinetics Modeling and Mechanism Analysis

To better understand and compare the adsorption behaviors of the biosorbents, the kinetic data were fitted using the intraparticle diffusion, pseudo-first-order, and pseudo-second-order models. These models provide insights into the rate-controlling mechanisms and the nature of the interactions between the adsorbate species (methyl red and Cu(II)) and the biosorbent surface.

5.1 Intraparticle diffusion model

The intraparticle diffusion model [25] helps elucidate whether diffusion within the pores of the

adsorbent is the rate-limiting step. The model is expressed as:

$$q_t = K_{int} t^{1/2} + \lambda \quad (2)$$

where q_t (μmol/g) is the adsorption capacity at time t, K_{int} (μmol/g·min$^{1/2}$) is the intraparticle diffusion rate constant, and λ (μmol/g) reflects the boundary layer thickness.

As shown in Fig. 3 and Table 4, the plots of q_t versus $t^{1/2}$ are multi-linear, indicating that the adsorption process occurs in two distinct stages.

The first stage (steeper slope) corresponds to film diffusion, where adsorbate molecules migrate from the bulk solution to the external surface of the biosorbent. The second stage (gentler slope) represents intraparticle diffusion within the pores of the adsorbent until equilibrium is reached.

The relatively high R^2 values (> 0.97) in the first stage for all biosorbents indicate that intraparticle diffusion significantly contributes to the overall rate but is not the sole rate-controlling step, as none of the plots pass through the origin ($\lambda \neq 0$). This deviation suggests the concurrent influence of boundary layer diffusion.

Among the biosorbents, MKB exhibited the highest K_{int} values for both MR and Cu(II), confirming a faster diffusion rate, likely due to its higher fixed carbon content and greater microporosity (see Table 2). This behavior aligns with reports by [5, 20], who observed enhanced diffusion in carbon-rich and well-activated lignocellulosic materials.

These results imply that the adsorption mechanism involves both surface adsorption and intraparticle diffusion, with the external mass transfer playing an important role, particularly in the initial phase.

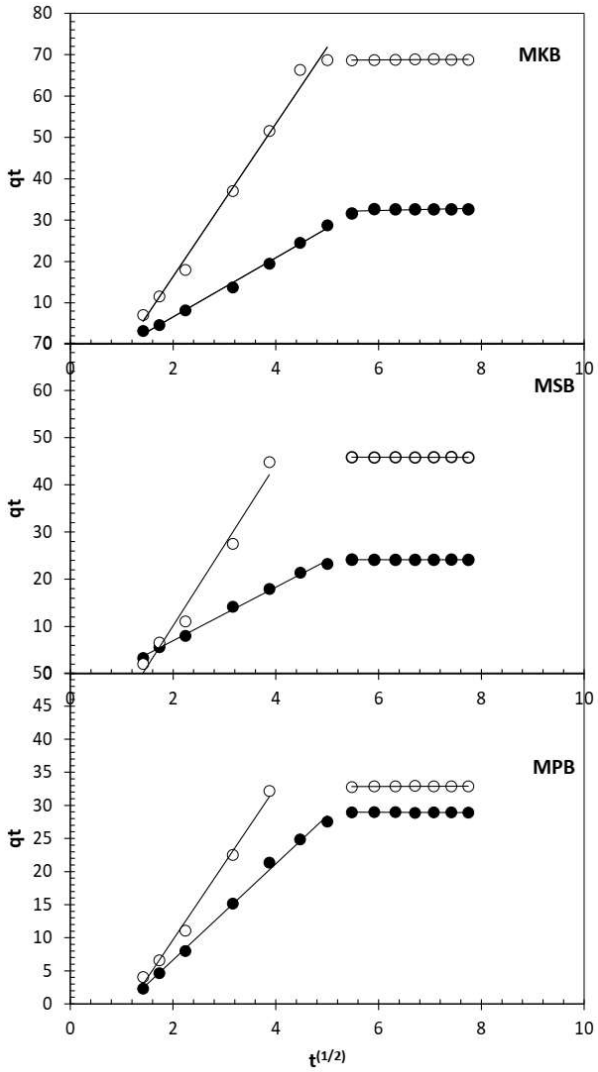

Fig. 3 Intraparticle plot for the adsorption of methyl red (•) and Cu(II) (o) on mango kerl biosorbent (MKB); mango seed biosorbent (MSB) and mango peels biosorbent (MPB).

Table 4 The intraparticle diffusion constant value of the adsorption of methyl red and Cu(II) on mango kerl biosorbent (MKB) ; mango seed biosorbent (MSB) and mango peels biosorbent (MPB).

Adsorbant	Polluant	Phase 1			Phase 2		
		$K_{int\,1}$ (μmol/g.min)	C_1	R^2_1	$K_{int\,2}$ (μmol/g.min)	C_2	R^2_2
MKB	RM	7.153	-7.718	0.995	0.288	30.581	0391
	Cu(II)	18.480	-20.61	0.990	0.075	68.281	0.309
MSB	RM	5.666	-4.343	0.996	-0.003	24.159	0.021
	Cu(II)	17.080	-24.009	0.977	-0.013	45.92	0.037
MPB	RM	7.263	-7.879	0.996	-0.028	29.128	0.313
	Cu(II)	11.526	-13.345	0.993	0.026	32.703	0.130

b. Pseudo-First-Order Model

The Lagergren pseudo-first-order kinetic model assumes that the rate of adsorption is proportional to the number of unoccupied sites:

$$log(q_e - q_t) = log(q_e) - \frac{K_1}{2.303}t \qquad (3)$$

Where K_1 (min^{-1}) is the pseudo-first-order rate constant.

As shown in Table 5, the correlation coefficients R^2 obtained for this model range from 0.67 to 0.84, indicating a poor fit compared to the pseudo-second-order model. Moreover, the calculated q_e values deviate considerably from the experimental ones.

Therefore, the pseudo-first-order model does not adequately describe the adsorption kinetics of MR and Cu(II) on the mango-derived biosorbents, suggesting that the adsorption is not solely governed by physical diffusion.

Similar discrepancies have been reported by [26, 27] for dye and metal ion adsorption onto agricultural waste-derived carbons, reinforcing that chemical interactions dominate the sorption process.

5.3 Pseudo-Second-Order Model

The pseudo-second-order kinetic model assumes that adsorption follows a chemisorption mechanism, involving electron sharing or exchange between adsorbate and adsorbent. It is expressed as:

$$\frac{t}{q_t} = \frac{1}{K_2 q_e^2} + \left(\frac{1}{q_e}\right)t \qquad (4)$$

where K_2 (g/µmol·min) is the rate constant and q_e (µmol/g) is the equilibrium adsorption capacity

Fig. 4 and Table 5 show that the pseudo-second-order model provides the best fit to the experimental data, with R^2 values typically above 0.93–0.98 and calculated q_e values close to the experimental ones. This strongly supports a chemisorption-controlled mechanism, involving valence forces through surface complexation and ion exchange between the active sites of the biosorbents and the adsorbate species.

The higher K_2 and q_e values observed for Cu(II) compared to methyl red suggest stronger interactions between metal ions and the oxygenated functional groups (–COOH, –OH, –C=O) present on the biosorbent surface, consistent with FTIR observations (Section 3.2.2).

Among the biosorbents, MKB again exhibited the highest adsorption capacity and rate constant, indicating that its surface characteristics (higher fixed carbon and functional group density) favor faster chemisorption.

These findings are consistent with those of [28-30], who observed pseudo-second-order behavior for simultaneous adsorption of dyes and metals on biomass-derived carbonaceous materials.

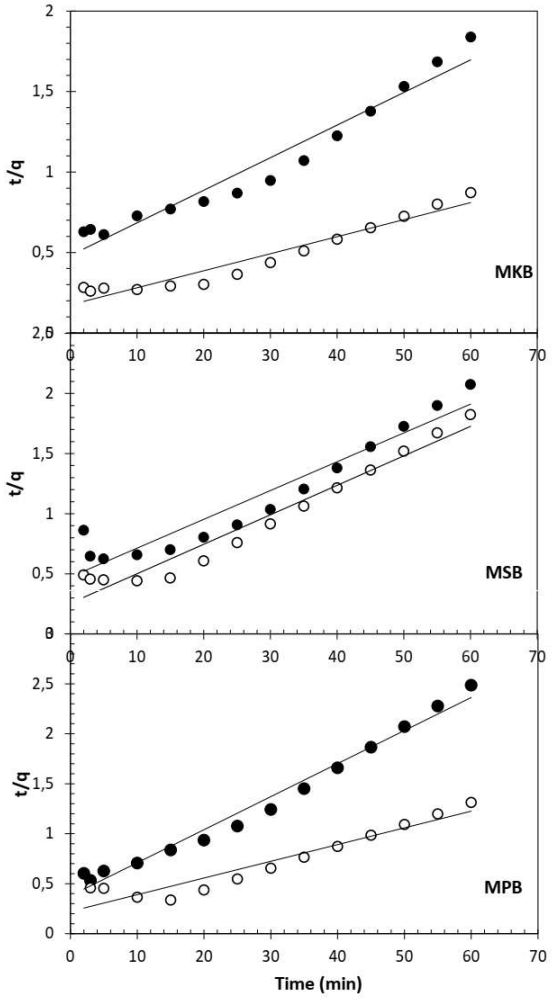

Fig. 4 Pseudo-second order plot for the adsorption of methyl red (•) and Cu(II) (o) on mango kerl biosorbent (MKB); mango seed biosorbent (MSB) and mango peels biosorbent (MPB)

Table 5 Pseudo-first and pseudo-second order kinetic model parameters for the adsorption of methylene red and Cu(II)

Adsorbant	Polluant	$q_{e\ Exp}$ (µmol/g)	Pseudo-premier ordre			Pseudo-second ordre		
			K_1 (µmol/g.min)	$q_{e\ cal}$ (µmol/g)	R^2	K_2 (µmol/g.min)	$q_{e\ cal}$ (µmol/g)	R^2
BCM	MR	48.952	0.012	61.320	0.843	0.001	49.261	0.950
	Cu(II)	95.541	0.144	62.244	0.753	0.001	94.340	0.937
BAM	MR	32.315	0.137	19.011	0.693	0.003	30.211	0.980
	Cu(II)	58.662	0.126	20.907	0.756	0.001	59.880	0.913
BPM	MR	40.647	0.133	23.807	0.674	0.001	41.667	0.914
	Cu(II)	42.346	0.114	13.053	0.723	0.002	40.816	0.957

The determination coefficients R^2, the amounts of MR and Cu(II) adsorbed at equilibrium and the rate constants of pseudo-first order and pseudo-second order have been determined and reported in Table 5.

6. Proposed Adsorption Mechanism

The adsorption of methyl red (MR) and Cu(II) ions onto mango kernel (MKB), mango seed (MSB), and mango peel (MPB) biosorbents can be explained through a multi-step mechanism involving several physicochemical interactions. Initially, the adsorbate molecules migrate from the bulk solution to the external surface of the biosorbent, a process known as film diffusion. The intraparticle diffusion plots indicate that this stage occurs rapidly, particularly for MR due to its larger molecular size, suggesting that boundary layer diffusion plays a significant role during the early phase of adsorption.

Following this, adsorbates penetrate into the internal pores of the biosorbents, a step identified as intraparticle diffusion. The multi-linear behavior of the q_t versus $t^{1/2}$ plots, along with non-zero intercepts, indicates that intraparticle diffusion is significant but not the sole rate-limiting step. The observed differences among biosorbents (MKB exhibiting higher adsorption rates compared to MSB and MPB) can be attributed to variations in porosity and surface area, which facilitate the diffusion of solutes into the pores.

Once inside the pores, chemisorption dominates the adsorption process, as confirmed by the superior fit of the pseudo-second-order kinetic model. Several interactions contribute to this chemisorption: ion exchange between Cu(II) ions and negatively charged surface groups such as carboxyl and hydroxyl groups, complexation or coordination with oxygenated functional groups identified by FTIR, and, in the case of MR, possible π–π interactions with aromatic lignin structures. The heterogeneous surfaces of the biosorbents allow partial simultaneous adsorption of MR and Cu(II), despite potential competition for active sites. Overall, Cu(II) ions show stronger adsorption than MR, likely due to their higher affinity for oxygen-containing functional groups, whereas MR adsorption may involve additional non-covalent interactions.

Therefore, the overall adsorption process can be described as chemisorption-dominated, with both intraparticle and boundary layer diffusion contributing to the rate control.

These observations are consistent with recent studies that report multi-step adsorption mechanisms for simultaneous removal of dyes and metal ions on lignocellulosic biosorbents [5, 26, 28-30].

7. Conclusion

The kinetic and mechanistic analysis of MR and Cu(II) adsorption onto mango-derived biosorbents demonstrates that the process involves multiple steps, including film diffusion, intraparticle diffusion, and chemisorption. The pseudo-second-order kinetic model provides the best description of the adsorption behavior, highlighting the importance of chemical interactions in controlling the adsorption rate. Intraparticle diffusion contributes significantly to the overall adsorption but is not the sole rate-limiting step, as evidenced by the

multi-linear q_t versus $t^{1/2}$ plots.

Among the biosorbents, mango kernel (MKB) exhibits the highest adsorption capacity and rate, likely due to its favorable surface chemistry and pore structure. Cu(II) ions generally show stronger adsorption compared to MR, reflecting their higher affinity for oxygenated functional groups, while MR adsorption is enhanced by additional π–π interactions.

Overall, the findings confirm that mango-derived biosorbents are effective and promising materials for the simultaneous removal of organic dyes and heavy metal ions, combining efficient diffusion processes with strong chemisorption mechanisms. This study underscores the potential of agro-industrial residues as sustainable and multifunctional adsorbents for environmental remediation.

Références Bibliographiques

[1] UNESCO 2023. United Nations World Water Development Report 2023: Partnerships and Cooperation for Water. Paris: UNESCO.

[2] Mateo-Sagasta, J., Marjani, Z., Turral, H., and Burke, J. 2021. Water pollution from agriculture: global review. FAO.

[3] Ahmad, M., Khan, S., and Hussain, A. 2022. "Recent Advances in Sustainable Biosorbents for Wastewater Treatment: A Review." *Journal of Environmental Chemical Engineering* 10 (1): 106945.

[4] Rofikoh, V., Zaman, B., and Samadikun, B. P. 2024. "The Potential of Commercial Biomass-Based Activated Carbon to Remove Heavy Metals in Wastewater – A Review." *Jurnal Ilmu Lingkungan* 22 (1): 132-41.

[5] Adebayo, M. A., Adewuyi, A. P., Oladipo, A. A., and Olusanya, T. O. 2023. "Valorization of Fruit Waste as Biosorbents for Water Decontamination: Recent Trends and Challenges." *Environmental Nanotechnology, Monitoring and Management* 20: 100778.

[6] Chen, X., Li, Y., and Zhang, H. 2022. "Lignocellulosic Biosorbents for Heavy Metal Removal: Insights into Mechanisms and Applications." *Bioresource Technology Reports* 19: 101101.

[7] Amadou S. G., Cheikh G., Kama A. B., Abdoulaye P., Diégane D. T., and Modou F. 2024. "Hevalent Chromium Cr (VI) Removal from Water by Mango Kernel Powder." *Journal of Materials Science and Chemical Engineering* 12: 84-103.

[8] Nadeem R., Manzoor Q., Iqbal M., and Nisar J. 2016. "Biosorption of Pb (II) onto Immobilized and Native Mangifera indica Waste Biomass." *J. Ind. Eng. Chem.* 35: 185-94.

[9] Qiang, W., Yunlong, W., Zi, Y., Wenqing, H., Lizhu, Y., Li, Z., and Xiaowu, H. 2022. "Efficient Removal of Pb(II) and Cd(II) from Aqueous Solutions by Mango Seed Biosorbent." *Chemical Engineering Journal Advances* 11: 100295.

[10] Malvin, M., Vusumzi, E., and Pakade, S. J. M. 2017. "Biosorption of lead (II) by chemically modified Mangifera indica seed shells: Adsorbent preparation, characterization and performance assessment." *Process Saf. Environ. Prot* 111: 40-51.

[11] Dilbagh, S., Sowmya, V, Abinandan, S., and Shanthakumar, S. 2017. "Removal of Malachite Green Dye by Mangifera Indica Seed Kernel Powder." *J. Inst. Eng. India Ser. A.*

[12] Khelifi, O., Mehreza, I., Younsi, M., Nacef, M., and Affoune, A. M. 2018. "Methyl Orange Adsorption on Biosorbent Derived from Mango Seed Kernels." *LARHYSS Journal* 34: 1-12.

[13] Yin, X., Xu, P., and Wang, H. 2024. "Efficient and Selective Removal of Heavy Metals and Dyes from Aqueous Solutions Using Guipi Residue-Based Hydrogel." *Gels* 10 (2): 142. https://doi.org/10.3390/gels10020142.

[14] Moyo, M., Ncube, L., and Maphosa, L. 2022. "Competitive Adsorption of Dyes and Metals on Agricultural Waste-Derived Adsorbents." *Environmental Science and Pollution Research* 29(15): 22389–402.

[15] Othmani, A., Ben Salem, R., and Ayadi, S. 2024. "Biosorption of Mixed Pollutants from Industrial Effluents Using Lignocellulosic Materials." *Chemosphere* 352: 143723.

[16] Goering, H. K., and Van Soest, P. J. 1970. "Forage Fiber Analyses (Apparatus, Reagents, Procedures and Some Applications)." *U. S. Agriculture Handbook 379.* Washington: U. S. Government Printing Office. (Sciepub)

[17] Sluiter A., Hames B., Ruiz R., Scarlata C., Sluiter J., Templeton D., and Crocker D. 2012. "Determination of Structural Carbohydrates and Lignin in Biomass: Laboratory Analytical Procedure (LAP)." Technical Report No. NREL/TP-510-42618, revised August 2012. Golden, CO: National Renewable Energy Laboratory.

[18] Li, J., Wang, Y., and Zhang, L. 2024. "Phosphoric Acid-Activated Biosorbents from Fruit Waste: Optimization, Characterization and Adsorption of Dyes and Metals." *Chemosphere* 354: 143875.

[19] Rao, N., Kumar, P., and Singh, R. 2023. "Characterization and Utilization of Mango Processing Waste for Sustainable Biosorbent Development." *Journal of Environmental Management* 345: 118634.

[20] Kurniawan, T. A., Gunawan, F., and Prasetyo, A. 2022. "Preparation and Physicochemical Characterization of

Fruit Peel Biosorbents for Wastewater Treatment." *Journal of Environmental Chemical Engineering* 10 (4): 107764.

[21] Abdelhafez, A. A., El-Sayed, G. H., and Hassan, M. F. 2021. "Surface Functionalization and Adsorption Behavior of Mango Peel-Based Biosorbents for Metal Ion Removal." *Environmental Science and Pollution Research* 28: 33245–33257.

[22] He, R., Hui, K., Zhang, X., and Yao, H. 2024. "Insight into the Role of the Pore Structure and Surface Functional Groups in Biochar on the Adsorption of Sulfamethoxazole from Synthetic Urine." *Applied Sciences* 14 (5): 1715.

[23] Hufton, J., Smith, R., and Taylor, P. 2021. "Surface Complexation and Competitive Adsorption Mechanisms of Heavy Metals on Biomass-Derived Adsorbents." *Environmental Science: Water Research & Technology* 7: 2118–31.

[24] Wang, Y., Liu, J., and Zhao, H. 2023. "Simultaneous Adsorption of Organic Dyes and Metal Ions on Modified Agricultural Waste Biosorbents." *Journal of Hazardous Materials Advances* 9: 100279.

[25] Weber, W. J., and Morris, J. C. 1963. "Kinetics of Adsorption on Carbon from Solution." *Journal of the Sanitary Engineering Division, American Society of Civil Engineers* 89 (2): 31-60.

[26] Ali, M. E., Hassan, S., and Rahman, A. 2021. "Kinetic Modeling of Heavy Metal Biosorption Using Lignocellulosic Residues." *Environmental Research* 200: 111707.

[27] Nguyen, H. T., Le, Q. T., and Pham, D. H. 2023. "Understanding Adsorption Mechanisms of Dyes on Biomass-Derived Adsorbents: A Kinetic and Thermodynamic Approach." *Journal of Hazardous Materials* 448: 131033.

[28] Gao, R., Li, Y., Zhang, H., and Chen, J. 2022. "Simultaneous Adsorption of Cationic Dyes and Heavy Metals Using Biochar: Kinetic and Mechanistic Perspectives." *Chemosphere* 298: 134321.

[29] Santos, J. R., Oliveira, P. F., and Costa, M. A. 2024. "Hybrid Biosorbents for Concurrent Dye–Metal Removal: Kinetic, Isotherm, and Mechanistic Analyses." *Separation and Purification Technology* 344: 125098.

[30] Sarkar, B., Ghosh, S., and Roy, P. 2021. "Biochar-based Adsorbents for Combined Removal of Organic and Inorganic Pollutants: A Kinetic Insight." *Bioresource Technology* 340: 125692.